

## Deactivation in Catalytic Hydrodemetallation

### III. Random-Spheres Catalyst Models

BARBARA J. SMITH<sup>1</sup> AND JAMES WEI

*Department of Chemical Engineering, Massachusetts Institute of Technology,  
Cambridge, Massachusetts 02139*

Received November 2, 1989; revised May 22, 1991

A "random-spheres" model is used to describe a porous catalyst, and to evaluate alternative postulates for the growth of metal-sulfide deposits in the catalyst during hydrodemetallation. The random-spheres model, unlike more common cylindrical-pore models, describes an interconnected three-dimensional pore space. Two alternatives are proposed for the form of the deposited metal-sulfides: a crystallite-deposits model and a uniform-deposits model. The crystallite-deposits model is shown to be more consistent with catalyst activity and catalyst characterization evidence for the form of metal-sulfide deposits. It can be used to predict changes in catalyst properties as metal-sulfide deposits accumulate, and can be applied to the industrially relevant case of diffusion-disguised metal deposition in catalyst pellets. © 1991 Academic Press, Inc.

#### 1. INTRODUCTION

Most models of deactivation in hydrodemetallation (HDM) catalysts have used a cylindrical-pore description of the catalyst-pore space and have modeled metal-sulfide deposits as accumulating in a uniform layer by layer manner inside the catalyst pore (1). These models may be inaccurate in two respects. First, the cylindrical-pore model of HDM catalysts is a simplification of the complex fine structure of porous materials. Second, there is no conclusive evidence that deposited metal sulfides coat the catalyst surface uniformly. In fact, the previous papers in this series (2) provide experimental evidence that deposited metal sulfides are present as spatially dispersed discrete crystallites.

van Eekelen (3) developed a more physically realistic model for porous catalysts based on randomly overlapping solid microspheres, the void being the remaining space between the microspheres. He used the ran-

dom-spheres model to examine the effects of a uniform layer of metal-sulfide deposits on catalyst deactivation. Reyes and Jensen (4) recently reviewed other statistical or stochastic models that have been used to describe catalyst-pore structure. Complex random pore network models have been developed as an extension of the cylindrical-pore approach. Other approaches include the simulation of porous solids as assemblages of spheres randomly arranged in space and distributed in size (5).

Discrete or crystallite-deposit models for the metal sulfides in HDM catalysts have been proposed previously. Smith and Wei (6, 7) discussed a purely random Poisson deposition process, and demonstrated that with discrete deposition of this type a significant fraction of the fresh catalyst surface area could remain uncovered in the presence of several monolayer-equivalents of deposits. If catalyst activity is related to the fraction of fresh catalyst surface exposed, this conclusion has obvious implications for the changes in catalyst activity as metal sulfides accumulate on the catalyst. Melkote and Jensen (8) recently compared uniform

<sup>1</sup> Present address: Chevron Research and Technology Company, Richmond, CA 94802.

and discrete deposition models, using a Bethe network to model the catalyst-pore space. Their results also indicate that discrete deposits permit fresh catalyst surface area to remain exposed at deposited metal loadings higher than those with uniform deposits.

In this paper the random-spheres model of van Eckelen is extended to describe not only the porous catalyst substrate, but also metal-sulfide deposits in the form of spatially dispersed crystallites. The objective is to develop a model that can be used to discriminate between the uniform and crystallite postulates for the form of metal-sulfide deposits, and can be used to predict changes in catalyst properties as metal-sulfide deposits accumulate.

## 2. RANDOM-SPHERES MODEL

In the random-spheres model (3, 9-11) for porous materials the porous solid is assumed to consist of a large number of randomly overlapping solid microspheres. This model differs from "packed-sphere" models in that it does not require that the sphere centers be at least one diameter from each other. Instead, the centers of the microspheres are randomly distributed in space, and the spheres are free to interpenetrate. The porous material is statistically homogeneous; that is, the properties of the material do not vary systematically with position. The model is illustrated in Fig. 1, which shows a cross section through a porous material comprised of randomly positioned spheres of equal size. The apparent distribution in diameters is due to the sectioning of spheres whose centers lie out of the sectioning plane. The void space between the solid microspheres is the pore space of the material.

The void fraction (void volume per unit volume),  $\psi$ , and surface area per unit volume,  $\Sigma$ , of a porous material comprised of monosize random spheres are uniquely determined by the two parameters of the random-spheres model: the number of sphere centers per unit volume,  $n$ , and the sphere

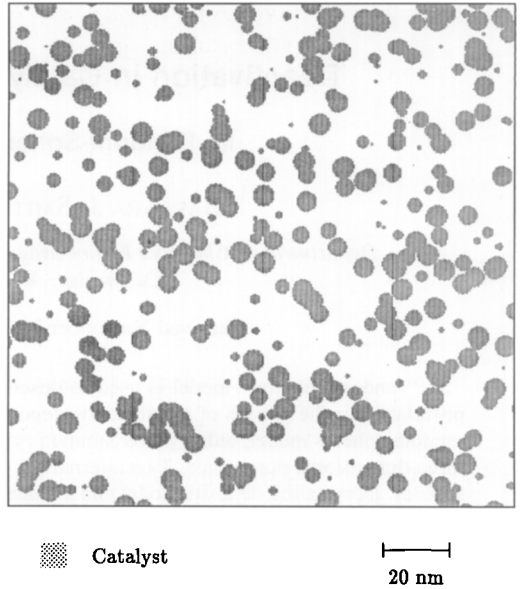


FIG. 1. Cross-sectional view of the random-sphere model of the CoMo/Al<sub>2</sub>O<sub>3</sub> catalyst. Catalyst-sphere radius:  $a = 3.27$  nm. Catalyst spheres per unit volume:  $n = 3.04 \times 10^{-3}$  nm<sup>-3</sup>. Catalyst-sphere clustering:  $\bar{v} = 3.6$ ,  $P_0 = 0.029$ . Void fraction,  $\psi = 0.64$ . (Specific surface area)  $\Sigma = 0.26$  nm<sup>-1</sup>. Pore-diameter distribution:  $\bar{d} = 6.6$  nm,  $\sigma_d = 2.2$  nm.

radius,  $a$  (see Appendix). Weissberg (9) derived the expression for  $\psi$  in the following manner.  $N$  sphere centers are placed at random in a finite volume,  $V$ . Since the placement of each center is independent of the positions of the other centers, the probability,  $P_v$ , that a smaller volume,  $v$ , contains no centers is

$$P_v = \left[ \frac{V-v}{V} \right]^N = \left[ 1 - \frac{nv}{N} \right]^N, \quad (1)$$

where  $n = N/V$ . As  $V$  and therefore  $N$  are made larger and larger, holding  $n$  and  $v$  fixed, the probability that  $v$  contains no centers become

$$P_v = \lim_{N \rightarrow \infty} \left[ 1 - \frac{nv}{N} \right]^N. \quad (2)$$

The void fraction,  $\psi$ , can be regarded as the probability that a random point is not contained by any solid sphere, or, equiva-

lently, as the probability that no sphere centers are within one sphere radius,  $a$ , of the random point. Thus, defining  $v = 4\pi a^3/3$  and writing  $\psi = P_v$

$$\psi = \exp\left[-\frac{4}{3}\pi na^3\right]. \quad (3)$$

Without consideration of overlap, the specific surface area of a system of  $n$  spheres per unit volume is  $4\pi na^2$ . The specific surface area of the overlapping random-spheres model is calculated using the fact that any random point has probability  $\psi$  of falling in the void space, and therefore only a fraction  $\psi$  of the surface has the probability of falling outside solid volume (10). The specific surface area is therefore

$$\Sigma = 4\pi na^2\psi. \quad (4)$$

Equations (3) and (4) can be combined to give the relationship by which the sphere radius,  $a$ , is uniquely defined for a monosize random-spheres model

$$a = -\frac{3\psi}{\Sigma} \ln \psi. \quad (5)$$

One useful property of the porous medium, which can be calculated using the random-spheres model is the pore-size distribution. van Eekelen (3) has presented the mathematical derivation for the pore-size distribution in a random-spheres model with arbitrary sphere-radius distribution. In this paper, van Eekelen's result has been used to calculate the mean pore diameter,  $\bar{d}$ , and the standard deviation of the pore-diameter distribution,  $\sigma_d$ , for all the presented random-spheres models.

The hydraulic pore-diameter,  $d_{hd}$ , which is by definition

$$d_{hd} = 4\frac{\psi}{\Sigma}, \quad (6)$$

can be calculated directly from

$$d_{hd} = \frac{1}{\pi na^2}. \quad (7)$$

At high enough sphere densities the ran-

dom-spheres model tends to generate clusters of overlapping spheres rather than a distribution of isolated spheres. At sufficiently low void fractions the random-spheres solid is a network material comprised of interconnected spheres. The mathematical description of this sphere clustering has been given by Haller (10). In the simple case of equally sized spheres, the mean number of other spheres,  $\bar{v}$ , by which a given sphere is intersected is just the mean number of centers of other spheres within a volume of radius  $2a$ . Therefore

$$\bar{v} = \frac{32}{3}\pi na^3. \quad (8)$$

Using the relationship given by Eq. (3)

$$\bar{v} = -8 \ln(\psi). \quad (9)$$

Haller (10) assumes a Poisson distribution around  $\bar{v}$ . The probability,  $P_v$ , for a sphere to have  $v$  intersecting neighbors is thus

$$P_v = \frac{\bar{v}^v}{v!} \exp(-\bar{v}) \quad (10)$$

or

$$P_v = \frac{[-8 \ln \psi]^v}{v!} (\psi)^8. \quad (11)$$

For a void fraction of 0.64, as depicted in Fig. 1, the mean number of touching neighbors for any given sphere,  $\bar{v} = 3.6$ . Less than 3% of all spheres are single and unattached; thus most, but not all, of the spheres are connected into a single continuous network or matrix.

The random-spheres model can be very simply extended by allowing a distribution of sphere radii. The generalized derivation is a straightforward repetition of the procedure used above for spheres of equal size (3). The simplest case is spheres of two discrete sizes; radii  $a_1$  and  $a_2$ , and number per unit volume  $n_1$  and  $n_2$ . The important results for this case are

$$\psi = \exp\left[-\frac{4}{3}\pi(n_1 a_1^3 + n_2 a_2^3)\right] \quad (12)$$

$$\Sigma = 4\pi(n_1 a_1^2 + n_2 a_2^2)\psi. \quad (13)$$

### 3. APPLICATION TO HYDRODEMETALLATION CATALYST DEACTIVATION

In this section we develop a random-spheres model to describe the catalyst used in the hydrodemetallation experiments and characterization studies reported in the previous papers in this series (2). This model is compared to a conventional cylindrical-pore model for the catalyst. Then alternative models for the growth of metal-sulfide deposits in the catalyst during hydrodemetallation are posed and evaluated. In Sections 3.2 and 3.3 the models are developed for catalysts aged without intraparticle mass-transfer limitations during hydrodemetallation. In Section 3.4 we apply them to the industrially relevant case of diffusion-disguised metal deposition in catalyst pellets.

#### 3.1 FRESH CATALYST MODELS

The catalyst modeled in this paper is American Cyanamid Aero HDS16A, the CoMo/Al<sub>2</sub>O<sub>3</sub> catalyst used in the experimental studies reported previously (2). The important properties of the catalyst are summarized in Table 1.

The simple cylindrical-pore model of unimodal pore-size distribution catalysts is used in this paper to provide a basis for comparison with the random-spheres catalyst model. The cylindrical-pore model, which has been used by many authors (12–15 and others), preserves the void fraction and specific surface area of the catalyst. Thus the diameter (or mean pore diameter in models with a distribution of pore diameters) of the model cylindrical pores is equal to the hydraulic-pore diameter of the catalyst.

The random-spheres model used to describe HDS16A has randomly overlapping solid microspheres of equal diameter. The two parameters of the random-spheres model, the number of sphere centers per unit volume,  $n$ , and the sphere radius,  $a$ , are specified according to Eqs. (4) and (5), using two properties of the porous catalyst, the void fraction,  $\psi_c$ , and the specific surface area,  $\Sigma_c$ . The sphere radius is 3.27 nm (32.7

Å) and number of spheres per unit volume is  $3.04 \times 10^{-3} \text{ nm}^{-3}$ .

The random-spheres model for HDS16A is illustrated in Fig. 1, which shows a cross section through the porous material. The apparent distribution in sphere diameters is due to the sectioning of spheres, the centers of which lie out of the plane. The mean number of spheres touched by a given sphere is 3.6, and the probability of any sphere being isolated is less than 3%. This suggests that the model is physically reasonable, in that most of the microspheres are physically connected to other microspheres. The most striking feature of Fig. 1 is the large void fraction (0.64), and the high degree of interconnectivity of the void volume. These factors are neglected in idealized cylindrical-pore models for these catalysts.

The random-spheres model preserves the hydraulic-pore diameter of the catalyst, 9.77 nm (97.7 Å), and provides a mean pore diameter of 6.6 nm (66 Å). The pore diameter distribution is close to normal in shape, with a standard deviation of 2.2 nm. The model sphere radius, 3.27 nm (32.7 Å) size can be compared with observations of the size of the alumina platelets that comprise HDS16A. As reported in the previous papers (2), transmission electron microscopy shows the alumina platelets to be rod-like, of approximate diameter 3 nm (30 Å), and length 25 nm (250 Å). A sphere of the same volume as the platelets has a radius of 3.5 nm (35 Å), which closely represents the sphere radius calculated for the random-spheres model.

#### 3.2. DEPOSITS MODELS

An extended random-spheres model is developed here to describe spatially nonuniform crystallite deposits in a porous catalyst. This model is compared to the case of uniform deposits in a cylindrical-pore catalyst, which has been considered previously by many authors (12–15 and others). It is also compared to a model of uniform deposits in a catalyst modeled using the random-spheres approach. Our development here is

TABLE I  
Parameters Used in Generating Catalyst Models

	Catalyst	
Pore volume		0.43 ml/g
Surface area		176 m <sup>2</sup> /g
Particle density		1.49 g/ml
Void fraction, $\psi$		0.64
Specific surface area, $\Sigma$		0.262 nm <sup>-1</sup>
Hydraulic pore diameter		9.77 nm
Random-spheres catalyst model		
Number of catalyst spheres per unit volume, $n_1$		$3.04 \times 10^{-3}$ nm <sup>-3</sup>
Catalyst-sphere radius, $a_1$		3.27 nm
Crystallite-deposits models		
Base case model (deposits on CoMo/Al <sub>2</sub> O <sub>3</sub> catalyst):		
Number of deposit spheres per unit volume, $n_2$		$4 \times 10^{-4}$ nm <sup>-3</sup>
Low $n_2$ case:		
Number of deposit spheres per unit volume, $n_2$		$4 \times 10^{-5}$ nm <sup>-3</sup>
Deposits on low-promoter/Al <sub>2</sub> O <sub>3</sub> catalyst:		
Number of deposit spheres per unit volume, $n_2$		$1.2 \times 10^{-5}$ nm <sup>-3</sup>
Relative specific activities:		
$\kappa_1$ (low-promoter Al <sub>2</sub> O <sub>3</sub> )/ $\kappa_1$ (CoMo/Al <sub>2</sub> O <sub>3</sub> )		0.05
$\kappa_2$ (Ni <sub>3</sub> S <sub>2</sub> )/ $\kappa_1$ (CoMo/Al <sub>2</sub> O <sub>3</sub> )		1.0
Uniform-deposits models		
Monolayer thickness		0.408 nm
Diffusion model		
Mean molecular diameter		1.17 nm

limited to the simple case of a flat metal deposition profile across the catalyst-particle radius, on a macroscopic scale (i.e., no intraparticle mass-transfer limitation during hydrodemetallation). In Section 3.4 we discuss extending the model to the mass-transfer limited case.

### 3.2.1. Pore Volume Effects of Metal-Sulfide Deposits

The first step in building a quantitative model of the effects of accumulating metal-sulfide deposits on the properties of a porous catalyst is to describe the changes in pore volume and void fraction. In the absence of coke deposits, total pore volume and void fraction depend only on the quantity of deposited metal and the relative densities of the fresh catalyst and the depositing species. We can write  $\psi'_c$ , the void fraction of the catalyst with deposits, as

$$\psi'_c = \psi - m_d \frac{\rho_c}{\rho_d} \quad (14)$$

where  $m_d$  is the deposit loading on a fresh catalyst basis (g deposit/g catalyst),  $\rho_c$  is the fresh catalyst particle density, and  $\rho_d$  is the deposit density. The pore volume depends upon the changing density of the catalyst as deposits accumulate. The density of the catalyst with deposits,  $\rho'_c$ , is given by

$$\rho'_c = \rho_c \left( 1 + m_d \frac{MW_{\text{metal}}}{MW_{\text{metal sulfide}}} \right) \quad (15)$$

and the pore volume of the catalyst with deposits,  $V'_p$ , by

$$V'_p = V_p \left[ \frac{\psi'_c / \rho'_c}{\psi_c / \rho_c} \right] \quad (16)$$

For our case the particle density of the catalyst, as received, is 1.49 g/ml. The den-

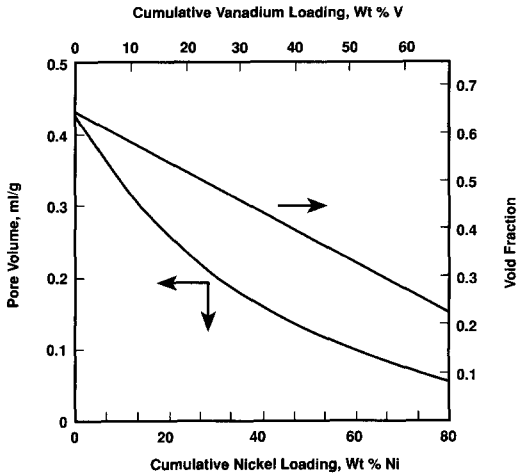


FIG. 2. Pore volume and void fraction versus cumulative metal loading, for all deposits models.

sity of  $\text{Ni}_3\text{S}_2$  is 5.82 g  $\text{Ni}_3\text{S}_2/\text{ml}$  or 4.27 g  $\text{Ni}/\text{ml}$ . The density of  $\text{V}_2\text{S}_3$  is 4.72 g  $\text{V}_2\text{S}_3/\text{ml}$  or 2.43 g  $\text{V}/\text{ml}$ . Figure 2 shows the linear decline in void fraction as a function of nickel or vanadium loading on the catalyst, for any deposit model. It also shows pore volume as a function of metal loading for the nickel-sulfide case. Since the pore volume depends on the average density of the catalyst, at a given void fraction the pore volume is slightly different in the nickel and vanadium cases. The catalyst pore volume declines to zero at a metal loading of 183 wt% Ni or 104 wt% V (on a fresh catalyst basis).

### 3.2.2. Uniform Deposits

The simplest possible model of the mode of metal-sulfide deposition is one in which the metal sulfides accumulate on the surface of the catalyst in a layer by layer manner, so that the solid catalyst substrate is uniformly coated with deposits. We apply this "uniform-deposits" model to both the cylindrical-pore and random-spheres catalyst models. The mathematical description of uniform deposits in a porous catalyst is straightforward. Only one parameter, the thickness of the deposit layer, needs to be

specified in order to calculate changes in catalyst properties such as void fraction and surface area. This is determined by the volume of deposits.

In a cylindrical-pore catalyst the deposit layer coats the walls of the cylindrical pores, continuously decreasing the pore-diameter loading as the thickness of the deposited layer increases. The thickness of the deposit layer for the cylindrical-pore model,  $\delta_{cp}$ , is derived by calculating the change in volume of a single cylindrical pore of radius  $r_p$ . It is

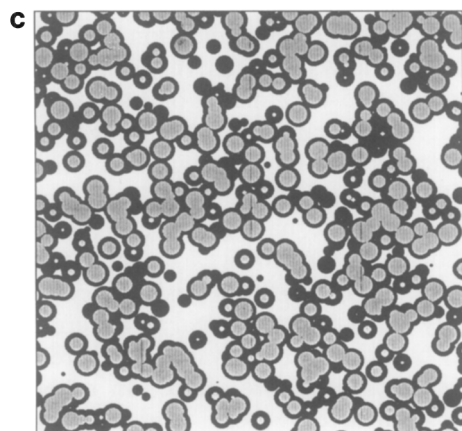
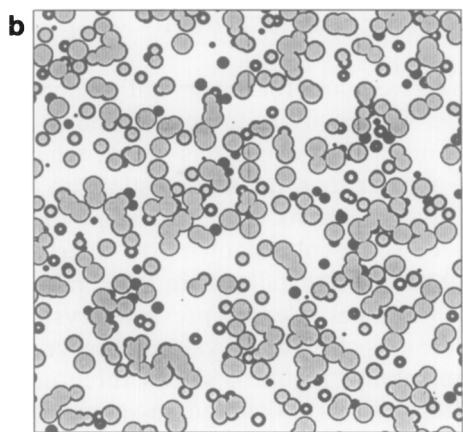
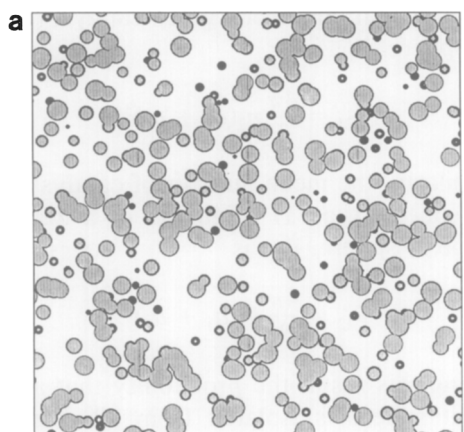
$$\delta_{cp} = (r_p - r'_p) = r_p \left[ 1 - \left( \frac{\psi'}{\psi} \right)^{1/2} \right]. \quad (17)$$



In a random-spheres catalyst model the deposit layer is allowed to coat the exterior of clusters of catalyst spheres. Thus the number density of catalyst spheres,  $n_1$ , is unchanged, and the radius of the spheres,  $a'_1$ , increases to account for the volume of deposits. With  $\psi'_c$  as the void fraction of the catalyst with deposits, using Eq. (3) we get that the thickness of the deposit layer,  $\delta_{rs}$ , is just

$$\delta_{rs} = (a'_1 - a_1) = \left[ -\frac{3}{4\pi n_1} \ln \psi' \right]^{1/3} - a_1, \quad (18)$$

where  $a_1$  is the radius of the catalyst substrate spheres. Calculating the volume of deposits in this manner accounts for the effects of overlap. The surface area and hydraulic pore diameter of the catalyst are given by Eqs. (4) and (7) using  $a'_1$  as the sphere radius.

Figure 3 shows three cross-sectional views of the random-spheres catalyst with uniform deposits at metal-deposition levels of 25, 50, and 100 wt% nickel, or equivalently 14, 29, and 57 wt% vanadium. The catalyst substrate is unaffected by the accumulation of deposits, which grow around "clusters" of catalyst substrate spheres, eventually causing clusters to merge as the pore space between them is filled. This is illustrated by the change in the value for  $\bar{v}$ , the mean number of catalyst spheres by



 Catalyst  
 Metal Sulfide Deposits

 20 nm

which a given sphere is intersected.  $\bar{v}$  increases from a value of 3.6 for the fresh catalyst to 9.9 at 100 wt% deposited nickel. In the mathematical model this is accomplished since in any region where the deposit layer potentially overlaps a neighboring catalyst sphere the overlap volume is still counted as catalyst substrate. The accumulation of metal sulfides results in a gradual loss of surface area and constriction of the catalyst pores. The mean pore diameter falls from 6.6 nm for the fresh catalyst to 5.1 nm at 100 wt% deposited nickel.

### 3.2.3. Crystallite Deposits

As discussed previously, the uniform-deposits model seems physically unreasonable in light of the HDM experiments and catalyst characterization studies reported by Smith and Wei (2). A more reasonable model is one that describes the metal-sulfide deposits as relatively large and spatially dispersed crystallites. The random-spheres approach provides us with a simple tool for developing such a model. The model is implemented by introducing a second set of spheres, representing the deposit phase, into the random-spheres-catalyst model developed in Section 3.1. Thus we use a random-spheres model with two discrete sphere types. The catalyst substrate is modeled using type 1 spheres. The added solid volume of the crystallite deposits is modeled using type 2 spheres. Any overlap between

FIG. 3. Cross-sectional view of the random-spheres model for uniform deposits at three metal loadings. (a) 25 wt% nickel or 14 wt% vanadium. (b) 50 wt% nickel or 29 wt% vanadium. (c) 100 wt% nickel or 57 wt% vanadium.

	(a) 25 wt% nickel, 14 wt% vanadium	(b) 50 wt% nickel, 29 wt% vanadium	(c) 100 wt% nickel, 57 wt% vanadium
Deposit layer:	$\delta_{rs} = 0.33$ nm	$\delta_{rs} = 0.64$ nm	$\delta_{rs} = 1.32$ nm
Sphere	$\bar{v} = 4.7$	$\bar{v} = 6.1$	$\bar{v} = 9.9$
clustering:	$P_0 = 0.009$	$P_0 = 0.002$	$P_0 = 0.0001$
Pore-diameter	$\bar{d} = 6.2$ nm	$\bar{d} = 5.8$ nm	$\bar{d} = 5.1$ nm
distribution:	$\sigma_d = 2.1$ nm	$\sigma_d = 2.0$ nm	$\sigma_d = 0.9$ nm

type 1 spheres and type 2 spheres is counted as belonging to material 1, so that the crystallite deposits effectively grow on and around the microspheres comprising the catalyst substrate material.

In order to calculate catalyst properties, two parameters need to be determined; the number of deposit spheres per unit volume,  $n_2$ , and the radius of the deposit crystallite spheres,  $a_2$ . In principle, any two independently observable catalyst properties could be used to specify these parameters. For the calculations presented in this paper we have estimated  $n_2$ , the number of deposit crystallites (type 2 spheres) per unit volume, from transmission electron micrographs of catalyst aged in nickel and vanadyl etioporphyrin hydrodemetallation (2). Using Eq. (12) the radius of the deposit (type 2) spheres,  $a_2$ , can then be calculated directly from the void fraction of the catalyst with deposits,  $\psi'_c$ ,

$$a_2 = \left[ -\frac{1}{n_2} \left( \frac{3}{4\pi} \ln \psi'_c + n_1 a_1^3 \right) \right]^{1/3}. \quad (19)$$

Some useful extensions to these equations can also be developed. The total surface area of the catalyst (exposed catalyst surface plus deposit surface) is given by Eq. (13), substituting  $\psi'_c$  for  $\psi$ . The fresh catalyst specific surface area (type 1 spheres) exposed in the presence of the deposit crystallites (type 2 spheres),  $\Sigma_1$ , is given by a simple extension of Eq. (13):

$$\Sigma_1 = 4\pi n_1 a_1^2 \psi'_c. \quad (20)$$

Using the sphere-clustering approach developed in Eqs. (8)–(11) we can calculate parameters that describe the degree of clustering in the material. The mean number of other deposit (type 2) spheres,  $\bar{v}_d$ , by which a given deposit sphere is intersected is just the mean number of centers of other type 2 spheres within a volume of radius  $2a_2$ . Therefore

$$\bar{v}_d = \frac{32}{3} \pi n_2 a_2^3. \quad (21)$$

The mean number of deposit (type 2)

spheres that intersect a given catalyst (type 1) sphere,  $\bar{v}_{21}$ , is

$$\bar{v}_{21} = \frac{4\pi}{3} n_2 (a_1 + a_2)^3. \quad (22)$$

Similarly, the mean number of catalyst microsphere (type 1) neighbors of a deposit (type 2) sphere,  $\bar{v}_{12}$ , is

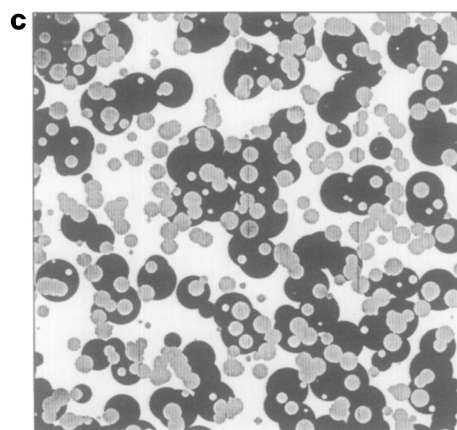
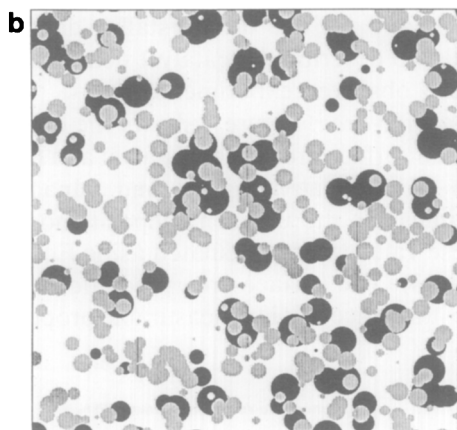
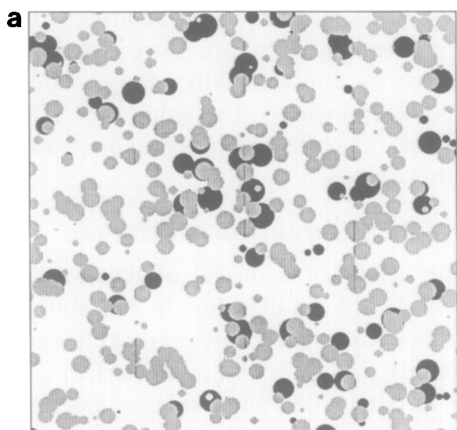
$$\bar{v}_{12} = \frac{4\pi}{3} n_1 (a_1 + a_2)^3. \quad (23)$$

Using this result the probability that a deposit sphere is isolated from all catalyst spheres,  $P_{d0}$ , can be calculated:

$$P_{d0} = \exp \left[ -\frac{4\pi}{3} n_1 (a_1 + a_2)^3 \right]. \quad (24)$$

As a base case for the crystallite-deposits model we specify  $n_2$  to be constant at  $4 \times 10^{-4} \text{ nm}^{-3}$ . We chose this value, which is 33% greater than the value estimated from TEM micrographs (2), to account for the loss of solid volume owing to overlap of neighboring crystallites in the random-spheres model. We thus preserve crystallite dimensions close to the values observed experimentally. Figure 4 shows three cross-sectional views of the random-spheres catalyst at metal deposition levels of 25, 50, and 100 wt% nickel, or equivalently 14, 29, and 57 wt% vanadium. The catalyst substrate is unaffected by the accumulation of deposits. Figure 4a shows the relatively small deposit spheres at 25 wt% nickel or 14 wt% vanadium. At higher metal loadings (Figs. 4b and 4c) the deposits have grown, and other deposit spheres, whose centers lie out of the sectioning plane, have grown into the cross-sectional view. At 100 wt% nickel or 57 wt% vanadium (Fig. 4c) the deposit spheres completely surround some catalyst spheres, entirely blocking the catalyst surface area and the surrounding pore space. In other regions, however, there are no deposit spheres, the catalyst surface is still exposed and the pore space is unconstricted. In this respect the crystallite-deposits model is fundamentally different from the uniform-de-





Catalyst

Metal Sulfide Deposits



20 nm

posits models presented in the previous section. The clustering of the deposit spheres is indicated by the values for,  $\bar{\nu}_d$ , the mean number of other deposit spheres by which a given deposit sphere is intersected.  $\bar{\nu}_d$  increases from 1.2 at 25 wt% nickel to 6.3 at 100 wt% nickel. The mean pore diameter is 6.6 nm in the fresh catalyst, the declines to 4.6 nm at 100 wt% deposited nickel.

The random-spheres model removes the constraint of a simplistic cylindrical-pores model. It demonstrates that, because of the high void fraction of these catalysts, the size of deposit crystallites need not be restricted to the nominal catalyst-pore diameter. The random-spheres crystallite-deposits model thus provides a ready explanation for the high-resolution electron microscopy observation, reported in Smith and Wei (2), that metal-sulfide crystallites are significantly larger than the nominal mean pore diameter of the catalyst. In a high void fraction material comprised of solid microspheres, a deposit phase can readily grow through the pore space and surround many substrate spheres, becoming much larger than the mean pore diameter.

In order to explore the impact of the model parameters of the crystallite-deposits model, we adjust the number of deposit spheres per unit volume down by an order of magnitude, so that at a given metal loading the deposit crystallites are much larger. Figure 5 shows the same cross-sectional view of the catalyst at 100 wt% nickel or 57

FIG. 4. Cross-sectional view of crystallite-deposits model base case, at three metal loadings. (a) 25 wt% nickel or 14 wt% vanadium. (b) 50 wt% nickel or 29 wt% vanadium. (c) 100 wt% nickel or 57 wt% vanadium.

	(a) 25 wt% nickel, 14 wt% vanadium	(b) 50 wt% nickel, 29 wt% vanadium	(c) 100 wt% nickel, 57 wt% vanadium
Deposit spheres:	$n_2 = 4 \times 10^{-4} \text{ nm}^{-3}$	$n_2 = 4 \times 10^{-4} \text{ nm}^{-3}$	$n_2 = 4 \times 10^{-4} \text{ nm}^{-3}$
Sphere:	$a_2 = 4.43 \text{ nm}$	$a_2 = 5.74 \text{ nm}$	$a_2 = 7.77 \text{ nm}$
clustering:	$\bar{\nu}_d = 1.2$	$\bar{\nu}_d = 2.5$	$\bar{\nu}_d = 6.3$
Pore-diameter distribution:	$P_{d0} = 0.003$	$P_{d0} = 0.0001$	$P_{d0} = 10^{-8}$
	$\bar{d} = 6.0 \text{ nm}$	$\bar{d} = 5.4 \text{ nm}$	$\bar{d} = 4.6 \text{ nm}$
	$\sigma_d = 20 \text{ nm}$	$\sigma_d = 1.7 \text{ nm}$	$\sigma_d = 1.2 \text{ nm}$

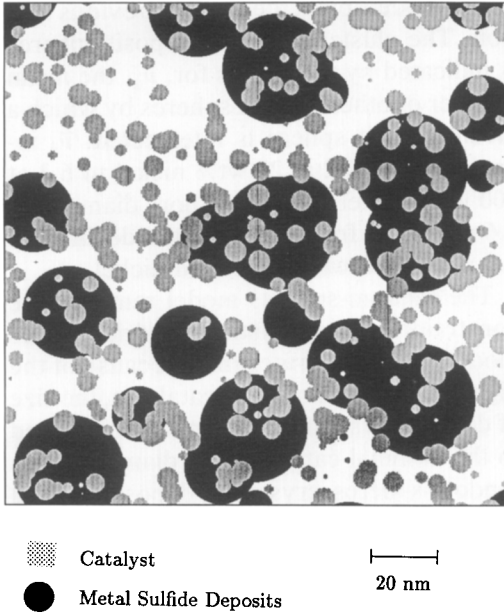


FIG. 5. Cross-sectional view of crystallite-deposits model, low number of deposit spheres per unit volume case.

100 wt% nickel, 57 wt% vanadium	
Deposit spheres:	$n_2 = 4 \times 10^{-5} \text{ nm}^{-3}$
	$\alpha_2 = 16.7 \text{ nm}$
Sphere clustering:	$\bar{v}_d = 6.3,$
Pore-diameter distribution:	$\bar{d} = 4.8 \text{ nm},$
	$P_{d0} = 10^{-45}$
	$\sigma_d = 1.2 \text{ nm}$

wt% vanadium for the case,  $n_2 = 4 \times 10^{-5} \text{ nm}^{-3}$ . The differences in deposit form between Figs. 4c and 5 are quite striking. In the low  $n_2$  case the deposit spheres are large enough to completely surround many catalyst spheres. The diameter of the deposits is clearly much larger than the pore diameter of the catalyst. Large regions of the catalyst are unaffected by the deposits.

In Fig. 6 crystallite-deposit (type 2 sphere) diameter is plotted as a function of cumulative nickel and vanadium loading. The base case,  $n_2 = 4 \times 10^{-4} \text{ nm}^{-3}$ , is shown to fit our experimental observations of nickel-sulfide and vanadium-sulfide crystallite-deposit size in the CoMo/Al<sub>2</sub>O<sub>3</sub> catalyst (2) very well. The crystallite deposits observed in a second catalyst, a low-pro-

porter Al<sub>2</sub>O<sub>3</sub> carrier, were relatively large and dispersed. These are more closely represented by a model with a lower value of  $n_2$ . As Fig. 6 shows, the value  $n_2 = 1.2 \times 10^{-5} \text{ nm}^{-3}$  fits our experimental observation for this system.

### 3.3 COMPARISON OF MODELS

The utility of a model of deposits in a porous HDM catalyst lies in the ability of the model to describe and predict changes in variables that affect catalyst performance, such as catalyst activity and transport properties. In this section we compare the predictions of the uniform- and crystallite-deposits models for some key catalyst properties, and we use the crystallite-deposits model to describe the catalyst deactivation results observed experimentally.

*Surface area.* Figure 7 shows the change in total surface area of the catalyst as a function of cumulative nickel and vanadium loadings for the different deposit models. These values were calculated using Eqs. (4) and (13). The surface area prediction is interesting since this is a measurable property.

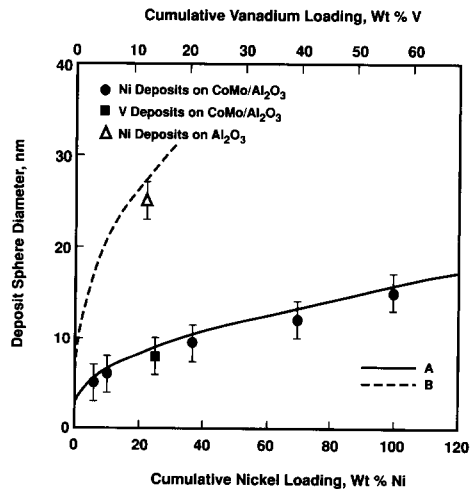


FIG. 6. Deposit-sphere diameter versus cumulative metal loading for crystallite deposits model. Catalyst modeled using random-spheres model. Data points are TEM observations (2). (A) Crystallite deposits, base case ( $n_2 = 4 \times 10^{-4} \text{ nm}^{-3}$ ), (B) Crystallite deposits, low  $n_2$  case ( $n_2 = 1.2 \times 10^{-5} \text{ nm}^{-3}$ ).

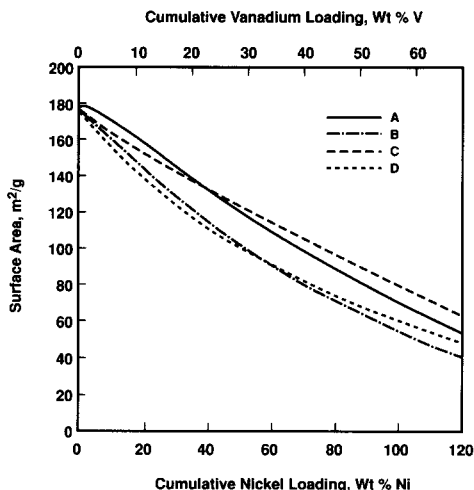


FIG. 7. Total surface area versus cumulative metal loading. (A) Crystallite deposits, base case ( $n_2 = 4 \times 10^{-4} \text{ nm}^{-3}$ ). Random-spheres catalyst model. (B) Crystallite deposits, low  $n_2$  case ( $n_2 = 4 \times 10^{-5} \text{ nm}^{-3}$ ). Random-spheres catalyst model. (C) Uniform deposits. Random-spheres catalyst model. (D) Uniform deposits. Cylindrical-pore catalyst model.

Comparison of the predictions for uniform deposits on the two different catalyst models shows that the cylindrical-pore model (D) overestimates the rate of surface area loss by up to 20% relative to the random-spheres model (C), because this simple description of the void space does not include the fact that real porous materials contain both convex and concave surface area elements.

When crystallite deposits are incorporated in the random-spheres catalyst model (A), the loss of surface area follows a somewhat different trend from that for uniform deposits (C,D). Initially there is a gain in surface area due to the growth of the deposit crystallites. As the crystallites coalesce and surround catalyst spheres, the catalyst loses surface area until at 100 wt% Ni or 57 wt% V the surface area of the catalyst is about one-third of the fresh catalyst value, and somewhat lower than in the case of uniform deposits in a random-spheres catalyst. Comparison of the second case of the random-spheres crystallite-deposits model (B), with

a smaller number of deposit crystallites per unit volume, shows a greater loss of surface area at a given deposited metal loading since some catalyst microspheres are completely surrounded by the deposit spheres, and the larger deposit spheres generate less new surface area.

Overall, the surface area predictions of the crystallite-deposits model are not significantly different from those of the model of uniform deposits in a random-spheres catalyst. This is because surface area is measured per mass of aged catalyst and the change in catalyst density, which is the same for all models, dominates the differences between the models. For this reason total surface area does not provide a sensitive test for discrimination between the uniform- and crystallite-deposits modes.

*Catalyst activity.* The crystallite-deposits and uniform-deposits models have very different implications for the impact of accumulating deposits on catalyst activity. These differences are highlighted in Fig. 8, which compares the fraction of the catalyst surface area that remains exposed as a function of cumulative nickel and vanadium

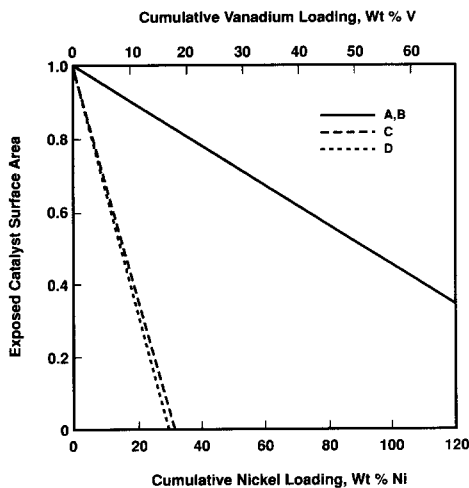


FIG. 8. Exposed catalyst surface area versus cumulative metal loading. (A,B) Crystallite deposits. Random-spheres catalyst model. (C) Uniform deposits. Random-spheres catalyst model. (D) Uniform deposits. Cylindrical-pore catalyst model.

loading. For the case of uniform deposits (C,D), the catalyst surface is completely masked once one monolayer-equivalent has been deposited. (Below one monolayer we assume that the fraction of catalyst surface exposed corresponds to the fraction of one monolayer-equivalent deposited.) In contrast, for crystallite deposits in a random-spheres catalyst (A,B) 86% of the catalyst surface remains uncovered with one monolayer-equivalent of deposits (32 wt% Ni or 18 wt% V). Approximately 45% of the catalyst surface is still exposed at a metal loading of 100 wt% Ni or 57 wt% V. This result, calculated according to Eq. (20), depends only on the volume of deposits, and is independent of the number of deposit spheres per unit volume. It demonstrates the potential for the active sites of the catalyst to continue to contribute to catalyst activity at relatively high metal loadings, if the deposit crystallites are not located preferentially on active catalyst sites.

In the first paper in this series (2) we reported on the impact of increasing levels of nickel-sulfide deposits on two catalysts with very different intrinsic activities. We found that both a sulfided CoMo/Al<sub>2</sub>O<sub>3</sub> catalyst and a low-promoter alumina carrier neither deactivated nor acquired catalytic activity as they accumulated nickel-sulfide deposits in model-compound HDM. These data are shown in Fig. 9. This result is inconsistent with a uniform mode of deposition because just one monolayer-equivalent of deposits (about 32 wt% Ni) would mask the intrinsic activities of the two catalysts. At higher metal loadings they would both show the same activity, reflecting the intrinsic activity of the deposited metal sulfide. The experimental result is consistent with a mode of nickel-sulfide deposition by which the active components of the catalyst continue to make a significant contribution to catalyst activity, even in the presence of high levels of deposited nickel sulfide. We apply the crystallite-deposits model to the aging of these two catalysts to examine how well this model can explain the experimental results.

A simple extension of Eq. (13) gives  $\kappa$ , the specific activity of the catalyst with crystallite deposits, as

$$\kappa = 4\pi\psi(\kappa_1 n_1 a_1^2 + \kappa_2 n_2 a_2^2). \quad (25)$$

$\kappa_1$  is the specific activity of the catalyst and  $\kappa_2$  is the specific activity of the nickel-sulfide deposits.

The parameters used in predicting catalyst activities with the crystallite-deposits model are given in Table 1. As discussed above, we estimated the random-spheres parameters ( $n_1, n_2, a_1$ ) from catalyst characterization studies, and calculated the deposit-sphere radius,  $a_2$ , directly from the deposited nickel loading using Eqs. (14) and (19). Further, we used experimental observations (2) to estimate the activity of the low-promoter alumina carrier relative to that of the CoMo/Al<sub>2</sub>O<sub>3</sub> catalyst (0.05). We assumed a value of 1.0 for the parameter ( $\kappa_2(\text{Ni}_3\text{S}_2) / \kappa_1(\text{CoMo}/\text{Al}_2\text{O}_3)$ ), to give a good fit of the model to the experimental data for both catalysts. (Interestingly, this suggests that the specific activity of nickel-sulfide deposits is the same as that of the CoMo/Al<sub>2</sub>O<sub>3</sub> catalyst.)

The solid lines in Fig. 9 are the predictions

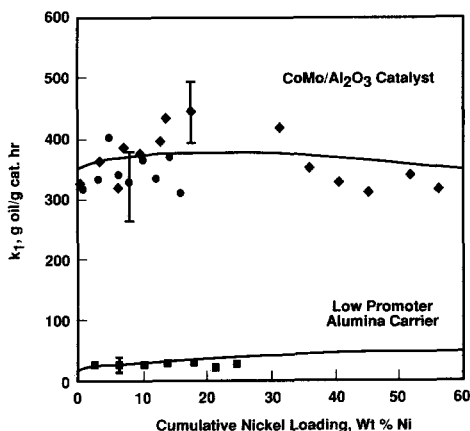


FIG. 9. Catalyst activity ( $k_1$ , hydrogenation rate constant for HDM) versus cumulative nickel loading on a CoMo/Al<sub>2</sub>O<sub>3</sub> catalyst and a low-promoter Al<sub>2</sub>O<sub>3</sub> carrier (2). Solid lines are predictions by the random-spheres crystallite-deposits model.

of the crystallite-deposits models for the CoMo/Al<sub>2</sub>O<sub>3</sub> catalyst and the low-promoter alumina carrier. For both catalysts, the models predict relatively steady catalyst activities up to deposited nickel loadings of 60 wt% Ni. The predictions fit the experimental data quite well. The low activity of the low-promoter alumina carrier is maintained to quite high deposited metal loadings because the relatively sparse, large nickel-sulfide crystallites observed in this catalyst generate a relatively small amount of high-specific-activity surface area.

*Effective diffusivity.* Percolation theory can be used to estimate transport coefficients in the porous media described by the various catalyst and deposit models. Macé and Wei (16) have investigated diffusion in a random-spheres catalyst model using the random-walk approach. In this paper we take a more simplistic approach based on the partitioning of molecules between bulk solution and porous solids. Limbach *et al.* (17) have addressed partitioning for a variety of molecule and pore shapes. They show that small molecule partitioning,  $\Phi$ , in granular materials is accurately represented by the simple expression

$$\Phi = (1 - d_m/d_{hd})^2, \quad (26)$$

where  $d_m$  and  $d_{hd}$  are the molecule and pore diameters respectively, provided that molecule size is characterized by mean projected diameter, and pore size by the hydraulic-pore diameter. Equation (26) becomes unreasonable only when a crucial pore dimension is of the same order of magnitude or smaller than the maximum linear dimension of the molecule. It is the basis of the correlation for diffusion in the restricted regime developed by Spry and Sawyer (18). The Spry-Sawyer correlation for effective diffusivity is

$$D_{\text{eff}} = \frac{D_b \psi}{\tau} \left[ 1 - \frac{d_m}{d_{hd}} \right]^4, \quad (27)$$

where  $D_b$  is the bulk diffusivity,  $\psi$  is the catalyst void fraction, and  $\tau$  is the catalyst

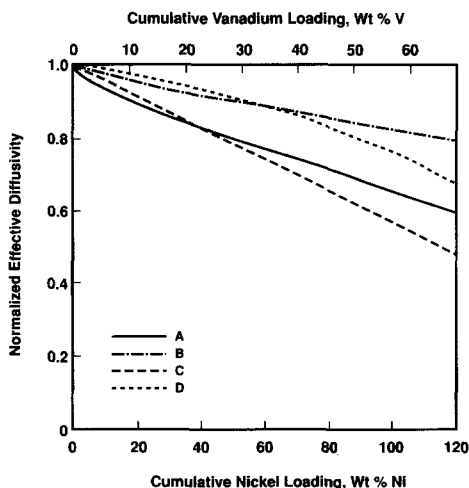


FIG. 10. Estimated effective diffusivity versus cumulative metal loading. (A) Crystallite deposits, base case ( $n_2 = 4 \times 10^{-4} \text{ nm}^{-3}$ ). Random-spheres catalyst model. (B) Crystallite deposits, low  $n_2$  case ( $n_2 = 4 \times 10^{-5} \text{ nm}^{-3}$ ). Random-spheres catalyst model. (C) Uniform deposits. Random-spheres catalyst model. (D) Uniform deposits. Cylindrical-pore catalyst model.

tortuosity. We use the orientation-averaged projected length to give a mean molecule diameter for the etioporphyrins of 1.17 nm. We expect catalyst tortuosity,  $\tau$ , to change as deposits accumulate in the catalyst. But, in the absence of any better information, in this paper the catalyst tortuosity is assumed to be invariant with the accumulation of deposits.

Figure 10 shows the change in normalized effective diffusivity as a function of cumulative metal loading. The model of uniform deposits in a cylindrical-pore catalyst (D) underestimates the loss in hydraulic pore diameter, and consequently overestimates effective diffusivity, relative to the model of uniform deposits in a cylindrical-pore catalyst (C). For the base-case crystallite-deposits model (A) effective diffusivity declines to 65% of the fresh catalyst value in the presence of 100 wt% nickel or 57 wt% vanadium. The differences in the predictions of the two alternative deposit models, uniform (A) and crystallite (C), in the random-spheres catalyst are not great, although the

crystallite-deposits model predicts a slightly higher effective diffusivity at high deposited metal loadings. The most striking result in Fig. 10 is that the second case of the crystallite-deposits model (B), with a low value for the parameter  $n_2$  and consequently a smaller number of larger deposit spheres, shows effective diffusivities that are 30% greater than the base-case crystallite-deposits model at high deposited metal loadings. This suggests that the coalescence of deposits into large crystallites might lead to a more active catalyst by increasing effective diffusivity. This result is confirmed by studies using percolation theory (16).

### 3.4 CRYSTALLITE DEPOSITS IN THE CASE OF INTRAPARTICLE MASS-TRANSFER LIMITATIONS DURING HDM

Our development of the crystallite-deposits model has been for the simple case of a flat metal deposition profile across the catalyst-particle radius, on a macroscopic scale (i.e., no intraparticle mass-transfer limitation during hydrodemetallation). In this section we discuss extending this model for application to a commercially aged HDM catalyst, in which there is typically a gradient in deposit loading across the catalyst-particle radius. This gradient corresponds to changes in the thickness of the deposit layer in the case of the uniform-deposits model, and to change in the number and/or size of the deposit crystallites in the crystallite-deposits model.

Figure 11 shows how the crystallite-deposits model can be extended for the mass-transfer limited case. In this representation, the number of deposit crystallites per unit volume (density of nucleation sites) is constant across the catalyst-particle radius, and the size of the crystallite deposits is highest toward the exterior of the catalyst pellet, corresponding to the maximum in the deposited-metal gradient. Macé and Wei (16) have applied such a model to the prediction of metal deposition profile in a catalyst pellet as a function of time.

## 4. DISCUSSION

The random-spheres model is readily applied to the description of crystallite deposits in a unimodal pore-size distribution catalyst. No adjustable parameters are used to reproduce the void fraction and surface area of the catalyst. In principle, any two independently observable catalyst properties could be used to specify the parameters describing the deposit crystallites. For the calculations presented in this paper we have estimated  $n_2$ , the number of deposit crystallites (type 2 spheres) per unit volume, from transmission electron micrographs of catalyst aged in nickel and vanadyl etioporphyrin hydrodemetallation (2). The radius of the deposit (type 2) spheres,  $a_2$ , is then calculated directly from the void fraction of the catalyst with deposits.

In evaluating the crystallite-deposits models we have adjusted the variable parameter, deposit sphere density,  $n_2$ , over an order of magnitude in order to assess the sensitivity of the calculated catalyst properties to these variables. This approach provides an interesting insight into the mode of deposition that is most favorable in terms of minimizing the restriction of reactant diffusivity as metal-sulfide deposits accumulate. If we had the ability to manipulate the density of deposit nucleation sites in the design of a hydrodemetallation catalyst, the most favorable design would be an extreme case in which there was one giant deposit sphere, and the remainder of the catalyst void was unaffected by deposits. The case depicted in Fig. 5, in which the number density of deposit crystallites is low, and consequently the size of the crystallites is relatively large, is an approach to this limit. The coalescence of deposits into large crystallites leads to a more active catalyst by increasing effective diffusivity. High-resolution electron microscopy (2) of two different catalysts aged in nickel etioporphyrin hydrodemetallation at the same conditions of temperature and pressure, showed significant differences in crystallite number and diameter. This sug-

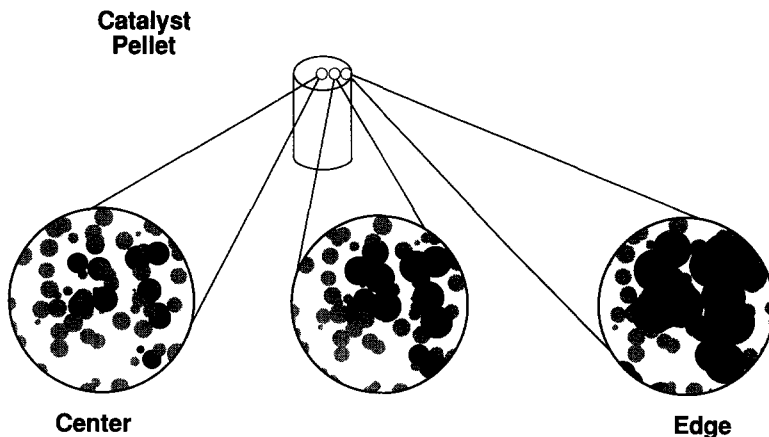


FIG. 11. Crystallite deposits in the case of mass-transfer limited metal deposition in a catalyst pellet.

gests that it may be possible to control crystallite-deposits distribution, and therefore the rate of catalyst deactivation, by controlling catalyst properties. However, whether crystallite number density can be controlled independently of catalyst activity is presently unknown.

One powerful feature of the random-spheres approach to modeling crystallite deposits is that it permits different scenarios for crystallite nucleation and growth mechanisms to be explored. In this paper we present a simple model in which the number of crystallites per unit volume is invariant, and increasing metal loading is accounted for by the growth of the deposit crystallites. This is equivalent to a simple nucleation and growth scenario in which crystallites nucleate initially at all sites, and then grow steadily. This simple scenario could be extended readily to account for simultaneous nucleation of new deposit crystallites and growth of existing crystallites throughout the life of the catalyst.

##### 5. CONCLUSIONS

In this paper a random-spheres model is used to describe a porous catalyst and to evaluate two alternative postulates for the form of metal-sulfides deposited in the catalyst during hydrodemetallation (uniform de-

posits and crystallite deposits). Our conclusions are as follows:

(1) The random-spheres model, unlike more common cylindrical-pore models, describes the catalyst as an interconnected three-dimensional pore space. The application of the random-spheres model to the description of a unimodal pore-size distribution catalyst is quite direct. No adjustable parameters are used to reproduce the void fraction and surface area of the catalyst. In the case evaluated here, the spheres that comprise the model material have the same characteristic dimension as the rod-like platelets of the real material. Thus the model is representative of the real material even at a microscopic scale.

(2) Experimental evidence from three sources, transmission electron microscopy, X-ray photoelectron spectroscopy, and catalyst activity studies, supports the crystallite-deposits model over the uniform-deposits model for catalysts aged in model compound hydrodemetallation at 320°C, 4.8 MPa (2). In keeping with the experimental observations, the crystallite-deposits model postulates a fixed number of deposit nucleation sites, and suggests initial nucleation of deposits is followed by growth of the crystallites at these sites. The predicted size of the deposit crystallites fits experimental ob-

servations by high-resolution electron microscopy very well. The random-spheres model removes the constraint of a simplistic cylindrical-pores model, and allows the deposited metal-sulfide crystallites to be significantly larger than the nominal mean pore diameter of the catalyst.

(3) The crystallite-deposits model is used to predict changes in catalyst properties as metal-sulfide deposits accumulate. Its predictions for surface area and catalyst coverage are compared to those of the uniform-deposits model. This comparison highlights the difference between the two models. In the case of uniform deposits the catalyst surface is completely masked once one monolayer-equivalent has been deposited, whereas for crystallite deposits a significant fraction of the catalyst surface remains uncovered in the presence of three monolayer-equivalents of deposits.

(4) The predictions of the crystallite-deposits model for changes in catalyst activity as a function of deposit loading (up to 60 wt% Ni) are shown to fit experimental data for two different catalysts. This comparison shows that the effect of metal-sulfide deposits on catalyst activity depends on the size and distribution, and therefore the exposed surface area, of the deposit crystallites, as well as on their intrinsic activity.

(5) The crystallite-deposits model suggests that if the density of deposit nucleation sites in a hydrodemetallation catalyst could be reduced without compromising catalyst activity, by manipulating process conditions or catalyst properties, a more active catalyst might be obtained since the effective diffusivity of metal-bearing molecules would be increased.

(6) The crystallite-deposits model can be applied to the industrially relevant case of diffusion-disguised metal deposition in catalyst pellets.

#### APPENDIX: NOMENCLATURE

$a, a_i$	Sphere radius, RSM
$\bar{d}$	Mean pore diameter, RSM
$d_{hd}$	Hydraulic pore diameter

$d_m$	Molecule diameter
$D_b$	Bulk diffusivity
$D_{eff}$	Effective diffusivity
HDM	Hydrodemetallation
$k_1$	Hydrogenation rate constant
$m_d$	Deposit loading (g deposit/g catalyst)
MW	Molecular weight
$n, n_i$	Number of sphere centers per unit volume, RSM
$N$	Number of sphere centers, used in derivation of RSM
$P_v$	Probability that a volume $v$ contains no sphere centers, used in derivation of RSM
$P_\nu$	Probability for a sphere to have $\nu$ intersecting neighbors, RSM
$P_{d0}$	Probability for a deposit sphere to have no intersecting catalyst neighbors, RSM
RSM	Random-spheres model
$r_p$	Pore radius
$V, v$	Volumes, used in derivation of RSM
$V_p$	Pore volume of catalyst (ml/g)
<i>Greek</i>	
$\delta_{cp}$	Thickness of uniform-deposit layer in cylindrical-pore model
$\delta_{rs}$	Thickness of uniform-deposit layer in random-sphere model
$\Phi$	Partition coefficient
$\kappa, \kappa_i$	Specific catalytic activity
$\nu$	Number of other spheres by which a given sphere is intersected, RSM
$\bar{\nu}$	Mean number of other spheres by which a given sphere is intersected, RSM
$\bar{\nu}_{12}$	Mean number of catalyst microsphere neighbors of a deposit sphere
$\bar{\nu}_{21}$	Mean number of deposit sphere neighbors of a catalyst microsphere
$\bar{\nu}_d$	Mean number of other deposit spheres by which a deposit sphere is intersected



$\Sigma$	Specific surface area
$\sigma_d$	Standard deviation of the pore size distribution, RSM
$\tau$	Catalyst tortuosity
$\psi$	Void fraction

*Superscript*

'	Catalyst with deposits
---	------------------------

*Subscripts*

<i>c</i>	Catalyst
<i>d</i>	Deposit
1	Type 1 sphere, catalyst
2	Type 2 sphere, deposit

## ACKNOWLEDGMENTS

The authors are grateful to Joe McIntyre, of the MIT Department of Brain and Cognitive Sciences, who made possible the graphics for the random-spheres models and to Olivier Ma e, of the Institut Fran ais du P trole, who assisted with computer calculations.

## REFERENCES

1. Quann, R. J., Ware, R. A., Hung, C. H., and Wei, J., *Adv. Chem. Eng.* **14**, 95 (1988).
2. Smith, B. J., and Wei, J., *J. Catal.* **132**, 1 and 21 (1991).
3. van Eekelen, H. A. M., *J. Catal.* **29**, 75 (1973).
4. Reyes, S., and Jensen, K. F., *Chem. Eng. Sci.* **40**, (191), 1723 (1985).
5. Abbasi, M. H., Evans, J. W., and Abrahamson, I. S., *AIChE J.* **29** (4), 617 (1983).
6. Smith, B. J., and Wei, J., "Catalyst Deactivation During the HDM of Ni Porphyrin over CoMo/Al<sub>2</sub>O<sub>3</sub>," presented at the AIChE National Meeting, Chicago, IL, November 1985.
7. Wei, J., in "Catalyst Design: Progress and Perspectives" (L. L. Hegedus, Ed.). Wiley, New York, 1987.
8. Melkote, R. R., and Jensen, K. F., *Chem. Eng. Sci.* **44** (3), 649 (1989).
9. Weissberg, H. L., *Appl. Phys.* **34**, 2636 (1963).
10. Haller, W. J., *Chem. Phys.* **42**, 686 (1965).
11. Streider, W. C., and Prager, S., *Phys. Fluids* **11**, 2544 (1968).
12. Newson, E., *Ind. Eng. Chem. Process Des. Dev.* **14**, 27 (1975).
13. Dautzenberg, F. M., Klinken, J. V., Pronk, K. M. A., Sie, S. T., and Wijffels, J. B., *ACS Symp. Ser.* **65**, 254 (1978).
14. Hughes, C. C., and Mann, R., *ACS Symp. Ser.* **65**, 201 (1978).
15. Rajagopalan, K., and Luss, D., *Ind. Eng. Chem. Process Des. Dev.* **18**, 459 (1979).
16. Mac e, O., and Wei, J., *Ind. Eng. Chem. Res.* **30**, 909 (1991).
17. Limbach, K. W., Nitsche, J. M., and Wei, J., *AIChE J.* **35** (1), 42 (1989).
18. Spry, J. C., and Sawyer, W. H., "Configurational Diffusion Effects in Catalytic Demetallation of Petroleum Feedstocks," presented at the AIChE Ann. Meeting, Los Angeles, November 1975.